Optimization and sensitivity analysis on axisymmetric motile microorganism flow of viscoelastic nanofluid over a spinning circular disk with a central composite model

Surender Ontela, Venkataramana Musala, Sameh E. Ahmed & Thirupathi Thumma

Published online: 24 Aug 2023.

Submit your article to this journal ⧉

View related articles ⧉

View Crossmark data ⧉

Taylor & Francis
Taylor & Francis Group

Check for updates

Optimization and sensitivity analysis on axisymmetric motile microorganism flow of viscoelastic nanofluid over a spinning circular disk with a central composite model

Surender Ontela[a] (iD), Venkataramana Musala[a,b] (iD), Sameh E. Ahmed[c,d] (iD), and Thirupathi Thumma[e] (iD)

[a]Department of Mathematics, National Institute of Technology Mizoram, Aizawl, India; [b]Department of Mathematics, Malla Reddy Engineering College, Telangana State, Hyderabad, India; [c]Department of Mathematics, Faculty of Science, Khalid University, Abha, King, Saudi Arabia; [d]Department of Mathematics, Faculty of Science, South Valley University, Qena, Egypt; [e]Department of Mathematics, B V Raju Institute of Technology, Narsapur, Medak, Telangana State, India

ABSTRACT

A robust statistical analysis is presented for the axisymmetric motile microorganism flow over a spinning disk. The bio-convective flow of non-Newtonian nanofluid over a circular stretching rotating disk is considered. As a novelty, the influence of thermal radiation and binary chemical reaction and activation energy are incorporated to enhance the study. The requisite transformation rules are adopted to get a suitable non-dimensional model of the problem under consideration. Further, traditional numerical technique with the help of shooting-based Runge-Kutta fourth-order is employed subject to the suitable surface conditions in the proposed model. The characteristics of these parameters affecting the flow phenomena are depicted through graphs. According to the physical interpretation of the results, the non-Newtonian parameter, in conjunction with the stretching parameter, does have a significant role in elevating the radial velocity profile. A faster chemical reaction rate causes a decrease in fluid concentration, and faster energy transmission is caused by thermal radiation. The higher degree of thermal radiation and the greater Biot number are associated with a considerable increase in the rate of heat transfer and also boost the temperature of the nanofluid. The rate of heat transmission is extremely sensitive to the Biot number. A robust statistical approach namely Response Surface Methodology based on a face-centered Central Composite Design model is prescribed for the optimized heat transfer properties using various factors. The regression analysis is conducted through analysis of variance and the sensitive analysis of these factors is also exhibited. The current numerical analysis has relevance in the bioengineering of organisms movement, gas turbines, processing of food, enzyme bio-metals, and oil recovery.

1. Introduction

The issue of fluid flow over a spinning disk is one of the basic problems in fluid dynamics, and it is one of the topics that attract a lot of attention in a variety of industrial and technical operations. The Coriolis effect, as opposed to the fluid inertia, may counteract the viscous forces

CONTACT Thirupathi Thumma ✉ thirupathi.thumma@gmail.com 🖃 Department of Mathematics, B V Raju Institute of Technology, Narsapur, Medak, 502313, Telangana State, India.

occurring on a fluid as it spins in a rotating disk system. According to this force, objects that are in motion appear to repel when viewed from a reference frame that rotates. The transport of heat in the existence of the Coriolis force has emerged as a topic of increasing significance in engineering, biomedical, and industrial applications. These kinds of fluid currents are specifically to be found in spinning machinery and lubrication, gas turbines, food processing technologies, electronic devices containing rotatory components, air cleaning machines, medical instruments, memory-saving devices, and rotating equipment. Homotopy analysis was used by Hee Doh et al. [1] to report on the heterogeneous and homogeneous responses in a nanofluid hydromagnetic flow in a rotating disk with a varying thickness in the presence of a suction or injection factor. Khan [2] took into account the (D-FM) Darcy-Forchheimer Model to investigate computationally the influence of entropy creation *via* an elongating spinning surface is subjected to a non-linear radiative flow of a viscous liquid saturated with composite particles in the occurrence of mixed convection and multi-slip situations. Using the RKF-45 technique, Mandal and Shit [3] explored the entropy of a viscosity nanofluid flowing hydromagnetically and convectively across a rotating porous disk with a stretching rate that varied with time and along the disk's radial direction. Nayak [4] used HAM to explore the 3D MHD stream and energy transport measurements as well as the viscous dissipation of nanofluid over a contracting surface. Recently, When there are large misalignments between the flow and the disk axis, Dinarvand and Nejad [5] used the three-stage Lobatto IIIa formula implemented in MATLAB to investigate the off-centered stagnation point stream of a hybrid silver and magnesium oxide nanofluid affecting a spinning disk. Local thermal non-equilibrium affects a stable, viscous and incompressible Ostwald-de-Waele nano-liquid across a spinning disk in a permeable medium, Ragupathi et al. [6] examined this effect using RKF combined with the shooting technique. Izady et al. [7] have reported on the stability study of a continuous two-dimensional boundary layer stream of a ferrite-copper oxide hybrid nanofluid hydromagnetic stream across an elongating permeable wedge with linear radiative heat flux effects. Algehyne et al. [8] explored the hydromagnetic flow of a convective combination of ethylene glycol and water with nanoparticles like silver and graphene across a spinning disk in the presence of thermal convection, thermal radiation, and heterogeneous and homogeneous chemical reactions using HAM. Sarangi et al. [9] study the heat transfer and Bödewadt stream properties of the ternary fluid stream with second-order slip across a stretched rotating disk considering the dissipation and thermal radiation effects. Dinarvand and Rostami [10]. put forth the numerical findings on the unsteady 3D squeezed transport of the ferrite-graphene oxide-water hybrid nanofluid within a rotating channel with two parallel and vertical sheets, where the bottom sheet is fixed, stretchable, and porous, whereas the top sheet has movement and non-permeable. A few important studies on bioconvective flow over a spinning disk may also be found in other articles (See Ahmed et al. [11], Shamshuddin et al. [12], and Humane et al. [13]).

The activation energy is an obligatory component that must be present for a chemical reaction to take place. The smallest amount of energy necessary for molecules or atoms to endure a chemical reaction is referred to as this energy. The Arrhenius activation energy is essential for the engineering of geothermal systems, oil emulsions, and the mechanics of water. Using the perturbation approach, Bestman [14] considered a natural convective stream to investigate the effects of (BCR) Binary Chemical Reactions in a porous material in 1990. He noted that the activation energy is the energy threshold that initiates the reaction of species; hence, reactants give rise to products. He also said that the activation energy is the energy barrier. Researchers from all around the world conducted studies on the influence of Activation energy and BCR for both Newtonian and non-Newtonian fluid cases, which were influenced by a variety of materials and geometrical configurations. Which includes, Nayak et al. [15] reported on the entropy analysis of the electromagnetism of CNT suspensions with optimized entropy production and cubic autocatalytic chemical reaction using the Xue model. Shafique et al. [16], considered an elongating sheet to investigate the three-dimensional non-Newtonian fluid stream with rotation effects; The

energy transfer on the cross movement of micropolar fluids across a thin needle traveling in a parallel flow, influenced by binary chemical reaction and Arrhenius activation energy, was shown by Mabood et al. [17] using the RKF-45 approach. very recently, Ijaz et al. [18] explored HAM analysis on Sisko fluid considering energy irreversibility effects through the rotating surface. When chemical reactions and heat production effects were present, Nayak et al. [19] used Kummer's function to investigate the transport of mass and energy in a boundary layer stream *via* a medium that is porous of an electrically conducting viscoelastic liquid exposed to a longitudinal magnetic field. The numerical findings of Chu et al. [20] study of a 2D incompressible laminar steady third-grade fluid stream across an elongating surface in the presence of gyrotactic microorganisms was presented using the Shooting technique. Hayat et al. [21] described the Jeffrey fluid flow boundary layer phenomenon with the convective hydromagnetic flow within an inclined sinusoidal permeable channel in the presence of hall currents. Convective flow within a parallel permeable tube was presented by Ahmed et al. [22] by employing HAM. In order to explore the EMHD flow of a Carreau nano liquid across a thin needle under Robinson's circumstances and the Arrhenius pre-exponential factor law where double stratification is important, Mabood et al. [23] used the RKF-45 approach. A few important studies on nanofluid flows with activation energy may also be found in other articles (See Jabeen [24], and Acharya et al. [25]).

Bioconvection is the name given to the macroscopic liquid convective movement that is created by the density gradient. This movement is brought about by a group swimming strategy used by gyrotactic motile organisms. As a result, particles with a lower density are moving to the surface of a liquid, where they will be more easily observed. These self-propelled gyrotactic bacteria led to bioconvection by swimming in a particular direction, which enhanced the fundamental density of the fluid. When present in nanofluid, microorganisms are more productive and can increase the rate of heat transmission. Researchers from a wide variety of fields are interested in the fluid transport phenomena that involve very small particles acting as microorganisms because of the potential applications that these findings could have in the fields of oil recovery, food processing, enzyme bio-metals, and bioengineering of species transport. computational methods to scrutinize the distinct influences of slip on an unsteady axisymmetric stream of magnetic Carreau nanoparticles and a cluster of freely moving microorganisms by Faiz et al. [26]. In a recent study, to model the bioconvection transport of nanofluid *via* a lubricated surface inhabited by swimming microorganisms, Alqarani et al. [27] made use of a preexisting MATLAB code to replicate the melting heat phenomena. For the Buongiorno model with the Runge-Kutta scheme and the shooting technique, Shafiq et al. [28] analyzed the nanofluid bioconvection through a spherical disk using artificial neural networks (ANNs). Dinarvand et al. [29] used FDM to explore dual solutions and conduct a stability study on the constant laminar MHD movement of a nanofluid mixture along the horizontal slender needle including radiation from heat. Wang et al. [30] published a study on the natural bio-convective flow of a Maxwell nanofluid across an exponentially extending surface with slip and convective boundary conditions. Over an angled radiative stretching cylinder, Mondal et al. [31] conducted an entropy investigation of the thermo solute stratification of a nanofluid flow, including gyrotactic microorganisms. They discovered that, under parametric modification, the viscosity models react slightly differently. The Brownian motion of particles in the model-I scenario is greater than in the model-II situation. When a flat surface is exposed to a stagnation-point flow of chemically reactive Oldroyd-B fluid, Cui et al. [32] investigated the non-similar characteristics of heat generation in bioconvection. OHAM was utilized by Ghasemian et al. [33] to study the unsteady 3D stagnation point viscoelastic flow of nanofluid around a circular cylinder involving sinusoidal radius change using the Buongiorno model. By employing the shooting approach the mass-based hybrid nanofluid stream is reported by Dinarvand et al. [34] to address the Jeffery-Hamel model, they considered the non-uniform channel stream with the multi-slip influences. Ali et al. [35] have used the Galerkin method to examine the effects of motile microorganisms and a Lorentz force on the hydromagnetic, transient

Blasius and Sakiadis flows. The implications of bio-convection for the Carreau nanofluid flow across a stretched cylinder as described by Song et al. [36] when melting phenomena and chemical reaction effects are present.

A mathematical and statistical technique known as the Response Surface Methodology (RSM) is used to investigate and improve the performance of a response variable whose values are dependent on several different important factors. It is possible to use RSM to fit an empirical complete quadratic model by making use of the response data that was produced based on the CCD model. The model may be used to figure out the optimal range of input factors, which will provide the best possible response function. A plethora of researchers reported a variety of investigations by approximating the response function *via* the use of the Design of experiments. Amongst many others, Mahanthesh et al. [37] a sensitivity analysis of the thermal transfer rate over a wedge surface using the RSM was explored, taking into account the principal slip mechanisms as well as an exponentially space-dependent heat source and a linear thermal source. Using Runge Kutta Fhelberg scheme, Saraswathy et al. [38] analyzed the behavior and sensitivity of the rate of heat transfer in a micropolar fluid flowing through an asymmetric channel heated by Newtonian heating at a constant surface temperature and also optimized the energy rate with RSM. The Central Composite Design model (CCD) with a face-centered approach in the RSM was adopted by Mahanthesh et al. [39] to optimize energy transfer over a wedge with ethylene glycol as base fluid and ZnO as metal oxide. The improvement of the thermal conductivity of nanofluids is achieved by aggregating nanoparticles, as shown by several researchers. The fractal size of the nanoparticle aggregation, however, will have a significant impact on the nanofluid's thermal conductivity. In this direction, by utilizing the Finite Difference Method (FDM) and the RSM with a CCD model, Rana et al. [40] explored the influence of Hall current, nanoparticle aggregation, on nanofluid stream through the rotatory disk and also over the heated circular tube, as reported by Mahanthesh et al. [41] Computational research by Rana and Gupta [42] on the rotatory dynamics of a nano liquid across a disk under Stefan blowing and multiple slips using the nonlinear density temperature (NDT) is reported. The authors also used the RSM to optimize the rate of energy and solute transmission in the spinning fluid stream. Recently, various works have reported experimental designs using RSM based on CCD models, such as conventional thermo-solute Marangoni mixed flow over a rotating disk by Mackolil and Mahanthesh [43], quadratic convective radiative rotating flow over a cone with the finite element method by Rana and Gupta [44], Fayyadh et al. [45] have reported on the activation energy of a Carreau fluid that transports magnetized nanoparticles through a permeable surface. and Rana and Akash [46] published an analysis of buoyancy-driven flow on a vertical cylinder.

The aforementioned literature confirms and to the best of the author's knowledge, off late little attention is given to the optimization and sensitivity analysis of the axisymmetric gyrotactic motile microorganisms flow over an elongating rotatory disk. However, recently Abbasi et al. [47] reported the effects of heat absorption on bioconvective nanofluid flow over a rotating disk with the Keller-Box Method, Mahanthesh et al. [48] applied the RKF-45 scheme in combination with the Shooting Technique to investigate the influence of corillids and Lorentz forces on nanofluid flow over rotating disk and Umair Khan et al. [49] numerically explored the Casson nanofluid with gold as metals and blood as base fluid through a spinning stretchable disk considering nonlinear radiative heat flux. All of these studies ignored the significance of Arrhenius activation energy and radiation influence on motile microorganism flow through the convective thermal surface. The novelty of the present investigation is to explore numerical optimization and sensitivity analysis on axisymmetric motile microorganism flow of viscoelastic nanofluid over a spinning circular disk with a central composite model by the presence of binary chemical reaction and thermal radiation forces. Thus, the current investigation aims to address the following specific objectives.
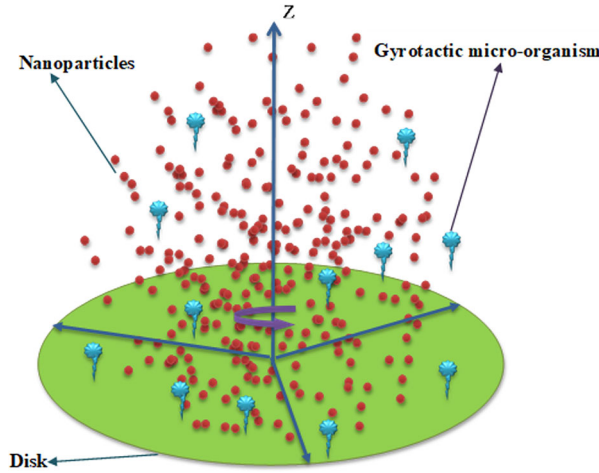
Figure 1. Schematic of flow configuration.

- The Buongiorno mathematical model is presented for the axisymmetric bioconvective visco-elastic gyrotactic microorganisms flow over a rotating circular disk subjected to a convective thermal surface and zero mass flux.
- The impact of the pertinent parameters such as Binary Chemical Reaction (BCR), heat source, thermophoresis, concentration of the fluid and motile particles, and thermal radiation on the flow configuration is explored.
- The multivariate fully quadratic model with three input factors for convective heat transfer coefficient using RSM is provided based on the Central Composite Design (CCD).
- Optimization levels of thermophoresis, thermal Biot number, and thermal radiation are determined and the sensitivity of the response function concerning physical input parameters is presented.

2. A Mathematical model for flow configuration

Considered here is the axisymmetric bioconvective flow of viscoelastic nanofluid across a circular disk spinning with an angular velocity Ω while being stretched in a radial direction at a constant rate S. Figure 1 depicts a physical sketch of the considered model by using cylindrical coordinates (r, θ, z) in such a manner that the disk is kept at a constant temperature T_w, the species concentration C_w is put at $z = 0$, and the fluid occupies the area $z > 0$. According to Revilin [50], the Cauchy stress tensor for the rheology of the fundamental flow field is defined as

$$\tau = -PI + \mu A_1 + \alpha_1 A_2 + \alpha_2 A_1^2 \tag{1}$$

In Eq. (1) the pressure is represented as P kinematic tensors are given as A_1 & A_2 and normal stress moduli are represented as α_1 & α_2. This article presents a comprehensive examination of the constraints imposed by these factors, and it is well known that it draws on research published by Dunn and Fosdick [51]. By ignoring the effects of body forces and doing a sub-sequential analysis based on the thermodynamic circumstances $\mu \geq 0$, $\alpha_1 \geq 0$ and $\alpha_1 + \alpha_2 = 0$, the governing balances of the flow are obtained as (See Abbasi et al. [47], Alqarani et al. [27], Chu et al. [20], Mahanthesh et al. [48] and Ghasemian et al. [33]).

$$\frac{\partial u}{\partial r} + \frac{u}{r} + \frac{\partial w}{\partial z} = 0 \tag{2}$$

$$\rho\left(u\frac{\partial u}{\partial r} + w\frac{\partial u}{\partial z} - \frac{v^2}{r}\right) = \frac{\partial \tau_{rr}}{\partial r} + \frac{\partial \tau_{rz}}{\partial z} + \frac{\tau_{rr} - \tau_{r\theta}}{r} \tag{3}$$

$$\left(u\frac{\partial v}{\partial r} - \frac{uv}{r} + w\frac{\partial v}{\partial z}\right)\rho = \frac{\partial \tau_{r\theta}}{\partial r} + \frac{2\tau_{r\theta}}{r} + \frac{\partial \tau_{\theta z}}{\partial z} \tag{4}$$

$$\left(u\frac{\partial w}{\partial r} + w\frac{\partial w}{\partial z}\right)\rho = \frac{\partial \tau_{zr}}{\partial r} + \frac{\partial \tau_{zz}}{\partial z} + \frac{2\tau_{rz}}{r} \tag{5}$$

$$u\frac{\partial T}{\partial r} + w\frac{\partial T}{\partial z} = \frac{k}{\rho c_p}\left(\frac{\partial^2 T}{\partial z^2} + \frac{\partial^2 T}{\partial r^2} + \frac{1}{r}\frac{\partial T}{\partial z}\right) + \tau\left[\frac{D_T}{T_\infty}\left\{\left(\frac{\partial T}{\partial r}\right)^2 + \left(\frac{\partial T}{\partial z}\right)^2\right\} + D_B\left(\frac{\partial C}{\partial r}\frac{\partial T}{\partial r} + \frac{\partial C}{\partial z}\frac{\partial T}{\partial z}\right)\right]$$
$$+ \frac{Q_0}{\rho C_p}(T - T_\infty) - \frac{1}{\rho C_p}\frac{\partial q_r}{\partial z} \tag{6}$$

$$u\frac{\partial C}{\partial r} + w\frac{\partial C}{\partial z} = \frac{D_T}{T_\infty}\left(\frac{\partial^2 T}{\partial z^2} + \frac{\partial^2 T}{\partial r^2} + \frac{1}{r}\frac{\partial T}{\partial r}\right) + D_B\left(\frac{\partial^2 C}{\partial z^2} + \frac{\partial^2 C}{\partial r^2} + \frac{1}{r}\frac{\partial C}{\partial r}\right)$$
$$- k_r^2(C - C_\infty)\left(\frac{T}{T_\infty}\right)^n \exp\left(\frac{-E_a}{kT}\right) \tag{7}$$

$$u\frac{\partial N}{\partial r} + w\frac{\partial N}{\partial z} + \frac{bW_c}{C_w - C_\infty}\left(\frac{\partial}{\partial r}\left(N\frac{\partial C}{\partial r}\right) + \frac{\partial}{\partial z}\left(N\frac{\partial C}{\partial z}\right)\right) = D_N\left(\frac{\partial^2 N}{\partial z^2} + \frac{\partial^2 N}{\partial r^2} + \frac{1}{r}\frac{\partial N}{\partial r}\right) \tag{8}$$

In Eqs. (2)–(8), The components of velocity in radial, azimuthal, and axial directions, are denoted with the dependent variables (u, v, w), motile microorganisms volume fraction is N, energy is T and solute concentration is C, τ_{rr}, $\tau_{\theta z}$, $\tau_{r\theta}$, τ_{rz}, τ_{zz} are the elements that make up the stress tensor of a fluid of the second grade, fluid density is ρ, heat flux of the thermal radiation is q_r, thermal conductivity of nanofluid k, the coefficient of thermophoretic diffusion is D_T, the motile micro particles species diffusivity is D_N, the coefficient of Brownian motion diffusion is D_B, chemotaxis constant is b and maximum cell spinning W_c.

Adopting the fundamental conduction rule, a simplified version of the slip conditions can be produced, and it is clear from several theoretical studies that using these circumstances enhances the heat conductivity at the wall's surface compared to using the no-slip conditions. Moreover, Nield and Kuznetsov [52] introduced the zero-mass flow condition that has also been taken into account. For the problem under consideration, the relevant constraints (See Abbasi et al. [47], Alqarani et al. [27], Kuznetsov and Nield [53]) at the disk's surface and the free stream are provided by

$$\left.\begin{array}{l} u(0) = Sr, \ v(0) = r\Omega, \ w(0) = 0, \ -k\frac{\partial T}{\partial z}(0) = h_w(T_w - T), \ \frac{\partial C(0)}{\partial z}D_B + \frac{\partial T(0)}{\partial z}\frac{D_T}{T_\infty} = 0, \ N(0) = N_w, \\ u(\infty) = 0, \ v(\infty) = 0, \ w(\infty) = 0, \ T(\infty) = T_\infty, C(\infty) = C_\infty, \ P(\infty) = P_\infty, N(\infty) = N_\infty \end{array}\right\} \tag{9}$$

Here coefficient of heat transfer is h_w the motile organisms concentration N_w, the temperature at the surface wall T_w, and the species concentration C_w.

Following Abbasi et al. [47] the linked PDEs were transformed into a set of ODEs using the set of similarity variables.,

$$\left.\begin{array}{l} \eta = z\left(\frac{2\Omega}{\upsilon}\right)^{1/2}, \ u = r\Omega f'(\eta), \ w = -f(\eta)\sqrt{2\upsilon\Omega}, \ \frac{N - N_\infty}{N_w - N_\infty} = \psi(\eta) \\ T - T_\infty = (T_w - T_\infty)\theta(\eta), \ C - C_\infty = (C_w - C_\infty)\phi(\eta), \ p = p_\infty - \Omega\mu p(\eta) \end{array}\right\} \tag{10}$$

Using Eq. (10) in Eqs. (3)–(8) we get,

$$f''' + \frac{g^2}{2} - \frac{f'^2}{2} + f''f + \alpha\left[2\left(g'\right)^2 + gg' - \left(f''\right)^2 - 2f'f''' - 2ff^{iv}\right] = 0 \tag{11}$$

$$g'' - f'g + fg' + \alpha\left[2f'g'' - gf''' - 2fg'''\right] = 0 \tag{12}$$

$$\theta'' + \frac{p_r}{(1+N)}\left[Nt\theta'^2 + \beta\theta + Nb\theta'\phi' + +f\theta'\right] = 0 \tag{13}$$

$$\phi'' + \frac{Nt}{Nb}\theta'' + Scf\phi' - \frac{1}{2}Sc\sigma_1(1+\delta\theta)^n\phi\exp\left(-\frac{E}{(1+\delta\theta)}\right) = 0 \tag{14}$$

$$\psi + L_b f\psi' - Pe\left[\psi'\phi' + Mc\phi'' + \psi\phi''\right] = 0 \tag{15}$$

Subject to,

$$\left.\begin{array}{l} f = 0, \quad f' = \lambda, \quad g = 1, \quad \theta' = -Bi_t(1-\theta), \quad \phi' + \frac{Nt}{Nb}\theta' = 0, \quad \psi = 1 \ at \ z = 0 \\ f' = 0, \quad g = 0, \quad f'' = 0, \quad g' = 0, \quad \theta = 0, \quad \psi = 0 \ at \ z \to \infty \end{array}\right\} \tag{16}$$

Where, Nb the Brownian motion parameter, Sc Schmidt number, p_r Prandtl number, Nt thermophoretic parameter, λ stretching parameter, β heat generation parameter, σ_1 chemical reaction constant, E activation energy parameter, δ temperature factor, Bi denotes the thermal Biot number, Pe (bioconvection) Peclet number, L_b (bioconvection) Lewis number, Mc microorganism-concentration constant, and α is a non-Newtonian fluid parameter.

$$p_r = \frac{\upsilon}{\alpha}, \quad Nt = \frac{D_T}{T_\infty}\frac{\tau}{\upsilon}(T_w - T_\infty), \quad Nb = D_B\frac{\tau}{\upsilon}(C_w - C_\infty), N = \frac{16\sigma^*}{3kk^*}T_\infty^3, Sc = \frac{\upsilon}{D_B},$$

$$\delta = \frac{(T_w - T_\infty)}{T_\infty}, \sigma_1 = \frac{k_r^2}{\Omega}, E = \frac{E_a}{k}, L_b = \frac{\upsilon}{D_N}, \quad Pe = \frac{bw_c}{D_N}, Mc = \left(\frac{N_\infty}{N_w - N_\infty}\right)$$

$$\lambda = \frac{S}{\Omega}, Bi = \frac{h_w}{k}\sqrt{\frac{\nu}{2\Omega}}, \beta = \frac{Q_0}{\Omega(\rho C_p)}$$

For this purpose, we define the local Nusselt and Sherwood numbers, which describe the heat and mass transfer on the disk's surface, and the local density number, which stands for the wall mass flow of the motile microorganisms.

$$Sh = \frac{r\frac{\partial C}{\partial z_{z=0}}}{C_w - C_\infty}, \quad Nu = \frac{r\frac{\partial T}{\partial z_{z=0}}}{T_w - T_\infty}, \quad De = \frac{r\frac{\partial N}{\partial z_{z=0}}}{N_w - N_\infty}. \tag{17}$$

In non-dimensional representation we have,

$$Re_r^{-\frac{1}{2}}Sh = \frac{Nt}{Nb}\theta'(0), \quad Re_r^{-\frac{1}{2}}Nu = -(1.0 + N)\theta'(0), \quad Re_r^{-\frac{1}{2}}De = \psi'(0). \tag{18}$$

3. Results and discussion

The axisymmetric motile microorganism flows over a spinning disk for the bio-convective flow of non-Newtonian nanofluid is considered in this analysis where the disk is stretching in a radial direction with uniform rate. The novel characteristic of a binary chemical reaction and activation energy is incorporated to enhance the study. The characteristic of the diversified constraints affecting the flow phenomena is organized by solving the modeled equations by using the shooting-based Runge-Kutta fourth-order technique. Therefore, the in-house routine code bvp4c in MATLAB is useful. The code validation is presented in Table 1 depicting the role of the

Table 1. Validation of the numerical results when $N = 0$, $\sigma_1 = 0 \& Bi = 0.1$.

	Abbasi et. al			Present Results		
α	$Re_r^{-0.5}Nu$	$Re_r^{-0.5}Sh$	$Re_r^{-0.5}De$	$Re_r^{-0.5}Nu$	$Re_r^{-0.5}Sh$	$Re_r^{-0.5}De$
0.1	0.065878381	−0.067587380	0.42297628	0.065878382	−0.067587381	0.42297624
0.3	0.071856782	−0.071856732	0.45239421	0.071856784	−0.071856735	0.45239423
0.5	0.074185529	−0.074185529	0.47345872	0.074185536	−0.074185528	0.47345877
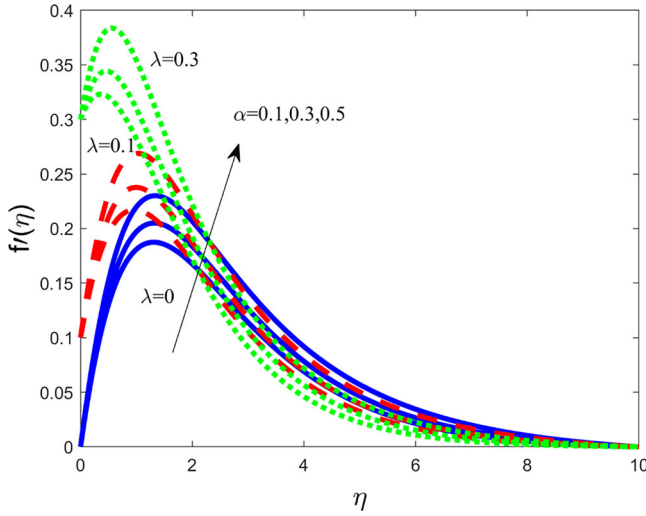
Figure 2. Profiles of $f'(\eta)$ at Pr $= 2$, Nt $=$ Nb $= 0.1$, n $= 1$, Sc $= 0.8$, $\delta = 0.5$, E $= 1$, Lb $=$ Pe $= 1$, Bi $= 0.1$, N $= 0.1$, Mc $= 0.1$, $\beta = 0.1$.

particular constraints $N = 0, \sigma_1 = 0 \& Bi = 0.1$ with different values of α for the Nusselt number, Sherwood number, and the local density number. The numerical results are correlates with the work of Abbasi et al. [40] that shows the convergence criteria as well as validation of the present result with the proposed methodology. The parametric behavior of the aforementioned parameters on the flow profiles is presented through Figures 2–15.

3.1. Variation of stretching and non-Newtonian parameters

Figure 2 describes the role of the stretching parameter combined with the non-Newtonian parameter on the radial velocity distribution. Here, $\alpha \neq 0$ indicates the properties of non-Newtonian fluid due to the relaxation time whereas $\lambda = 0$ shows the sheet is at rest and $\lambda \neq 0$ represents the case of stretching of the sheet. One of the peculiar characteristics is observed near the sheet region and it is seen that a sudden hike in the velocity profile occurred for the increasing stretching parameter irrespective of the variation of the non-Newtonian constraints. Further, the profile is dominated to reduce significantly as the domain increases. For $\lambda = 0$, when the sheet is at rest, the velocity profile retards significantly in comparison to the case of stretching. The augmented non-Newtonian parameter favors enhancing the velocity profiles and then ceases to requisite boundary conditions asymptotically. Figure 3 depicts the significant behavior of the non-Newtonian parameter and the stretching parameter on the nanofluid temperature. The comparative study reveals that increasing stretching restricts the fluid temperature vis-à-vis the thickness of the thermal bounding surface decreases significantly. Also, the non-Newtonian properties of the fluid decelerate the temperature significantly for their increasing values. Figure 4 illustrates the effects of the stretching parameter and the non-Newtonian parameter on the concentration
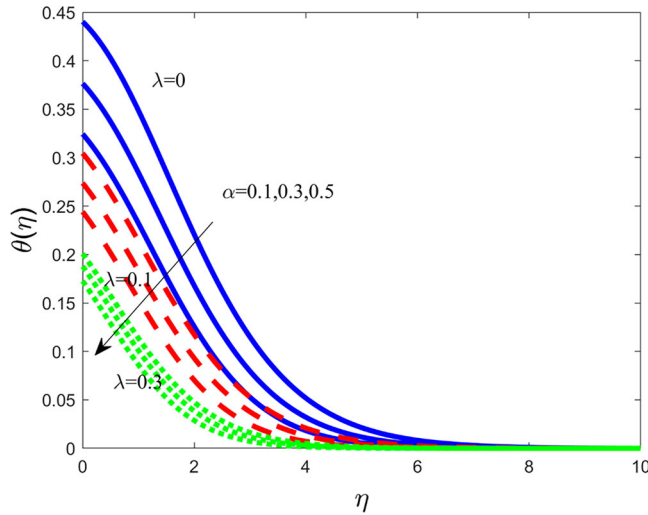
Figure 3. Profiles of $\theta(\eta)$ at Pr $=$ 2, Nt $=$ Nb $=$ 0.1, n $=$ 1, Sc $=$ 0.8, $\delta = 0.5$, E $=$ 1, Lb $=$ Pe $=$ 1, Bi $=$ 0.1, N $=$ 0.1, Mc $=$ 0.1, $\beta = 0.1$.
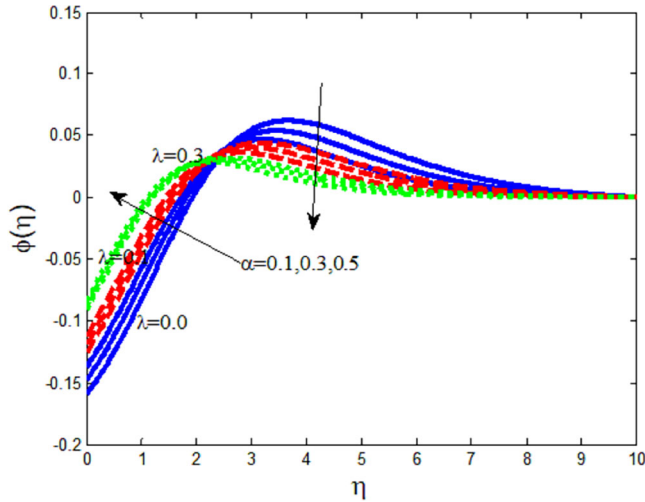
Figure 4. Profiles of $\phi(\eta)$ at Pr $=$ 2, Nt $=$ Nb $=$ 0.1, n $=$ 1, Sc $=$ 0.8, $\delta = 0.5$, E $=$ 1, Lb $=$ Pe $=$ 1, Bi $=$ 0.1, N $=$ 0.1, Mc $=$ 0.1, $\beta = 0.1$.

distribution. In an interesting observation, the dual characteristic in the profile is exhibited from the point of contact within the domain nearly $\eta = 2.5$. It is seen that, for the enhanced stretching the profile boosts up to increase the fluid concentration in the first region however, afterward it attenuates smoothly. The physical significance of the non-Newtonian parameter also corroborates with similar effects. Figure 5 contributes the effects of the non-Newtonian parameter as well as the stretching parameter on the motile-micro-organism profile. Though both the parameters attenuate the profile significantly it reveals an asymptotic behavior to meet the requisite boundary condition therefore, the strength retards the thickness of the bounding surface. Figure 6 depicts the significant characteristic of these parameters on the transverse velocity distribution for the existence of the other contributing coefficients as prescribed in the figure caption. The behavior shows distinct in nature concerning the radial velocity due to the rotational motion of the particles within the domain. The nonexistence of the stretching performs its maximum strength
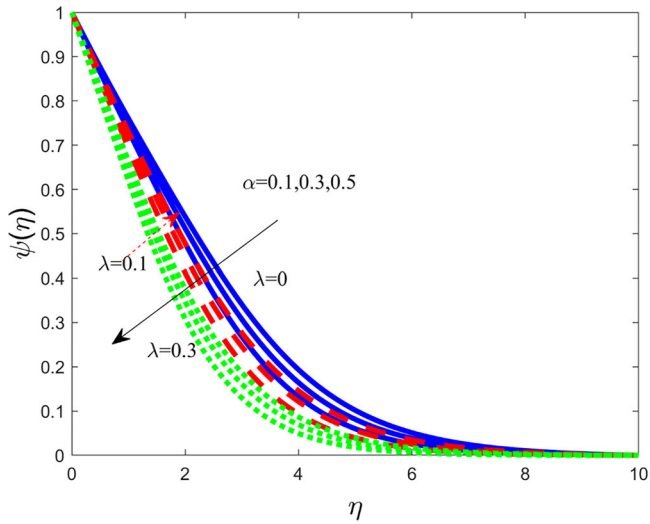
Figure 5. Profiles of $\psi(\eta)$ at Pr $=$ 2, Nt $=$ Nb $=$ 0.1, n $=$ 1, Sc $=$ 0.8, $\delta=0.5$, E$=$1, Lb$=$Pe $=$ 1, Bi $=$ 0.1, N$=$0.1, Mc $=$ 0.1, $\beta=0.1$.
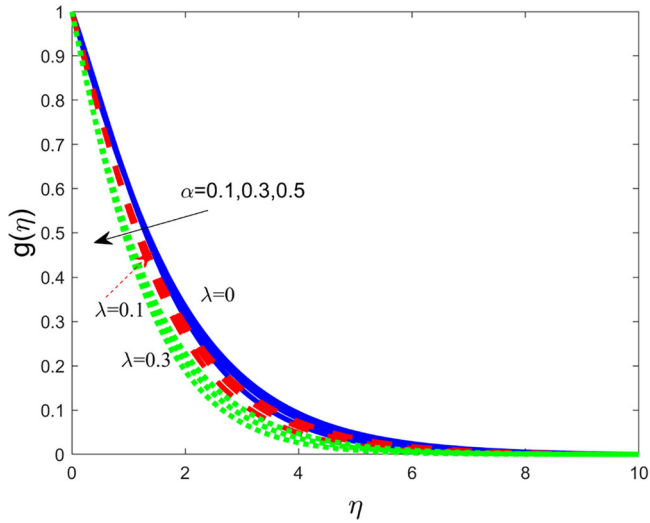
Figure 6. Profiles of g(η) at Pr $=$ 2, Nt $=$ Nb $=$ 0.1, n $=$ 1, Sc $=$ 0.8, $\delta=0.5$, E$=$1, Lb$=$Pe $=$ 1, Bi $=$ 0.1, N$=$0.1, Mc $=$ 0.1, $\beta=0.1$.

however the enhanced values retard the profile, and it became smooth with increasing domain to cease to zero. Further, the non-Newtonian relaxation parameter also favors in retarding the transverse velocity. These above-mentioned features have significant characteristics in recent technologies used in several industrial as well as engineering and electronic products to strengthen efficiency.

3.2. Effect of chemical reaction

Figure 7 illustrates the impact of binary chemical reactions due to the involvement of the activation energy on the concentration distribution. The numerical value $\sigma_1 = 0$ suggests the nonexistence of the chemical reaction coefficients whereas $\sigma_1 \neq 0$ indicates the role of various gaseous species affecting the concentration profile. The profile exhibited in the corresponding figure
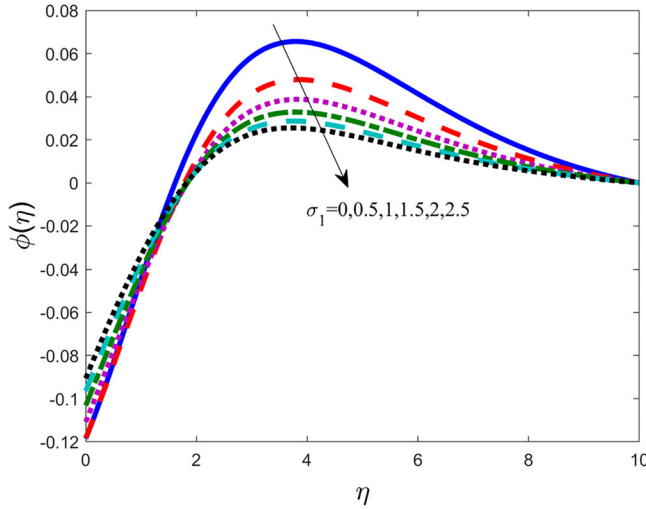
Figure 7. Profiles of $\phi(\eta)$ at Pr $= 1$, $\alpha = 1$, Nt $=$ Nb $= 0.1$, n $= 1$, Sc $= 0.8$, $\delta = 0.5$, E $= 1$, Lb $=$ Pe $= 1$, 03BB $= 0.2$, Bi $= 0.1$, N $= 0.1$, Mc $= 0.1$, $\beta = 0.1$.
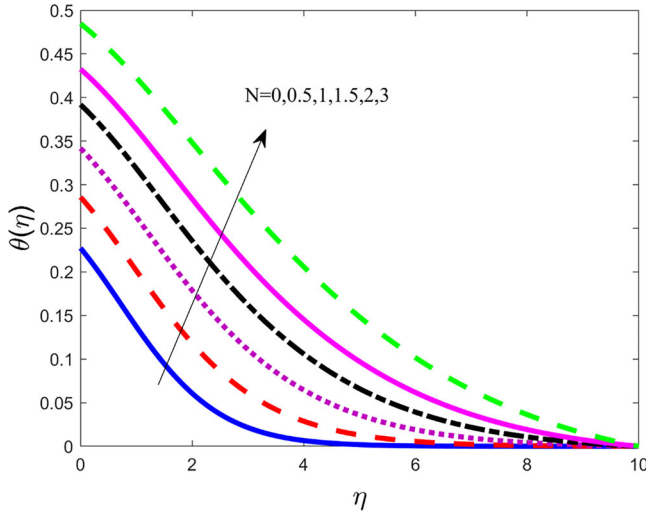

Figure 8. Profiles of 03B8(η) at Pr $= 2$, $\alpha = 0.1$, Nt $=$ Nb $= 0.1$, n $= 1$, Sc $= 0.8$, $\delta = 0.5$, E $= 1$, Lb $=$ Pe $= 1$, 03BB $= 0.2$, Bi $= 0.1$, N $= 0.1$, Mc $= 0.1$, $\beta = 0.1$.

reveals its dual characteristic and it is depicted that with an increasing chemical reaction the fluid concentration shows its sudden hike near the sheet region till the profiles have a point of inflection nearly about $\eta = 2$ and thereafter reverse impact is rendered. Therefore, the fluid concentration decelerates with enhanced reacting species contributing sooth behavior to achieve the prescribed free stream conditions.

3.3. Variation of thermal radiation

Figure 8 exhibits the influence of the radiating heat due to the conjunction of heat flux with the consideration of the Roseland approach affecting the nanofluid temperature. Thermal radiation is used as a measure of the amount of emission of electromagnetic radiation from the surface of the elements. Further, this emission will transform into thermal radiation. The mathematical
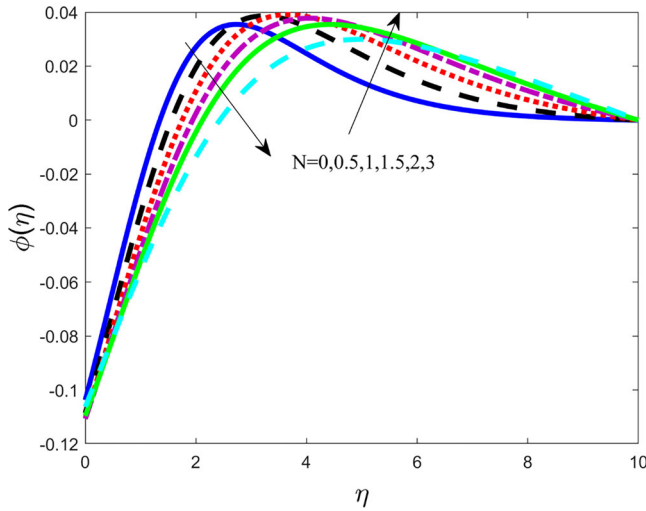
Figure 9. Profiles of $\phi(\eta)$ at Pr $= 2$, $\alpha = 0.1$, Nt $=$ Nb $= 0.1$, n $= 1$, Sc $= 0.8$, $\delta = 0.5$, E $= 1$, Lb $=$ Pe $= 1$, 03BB $= 0.2$, Bi $= 0.1$, N $= 0.1$, Mc $= 0.1$, $\beta = 0.1$.
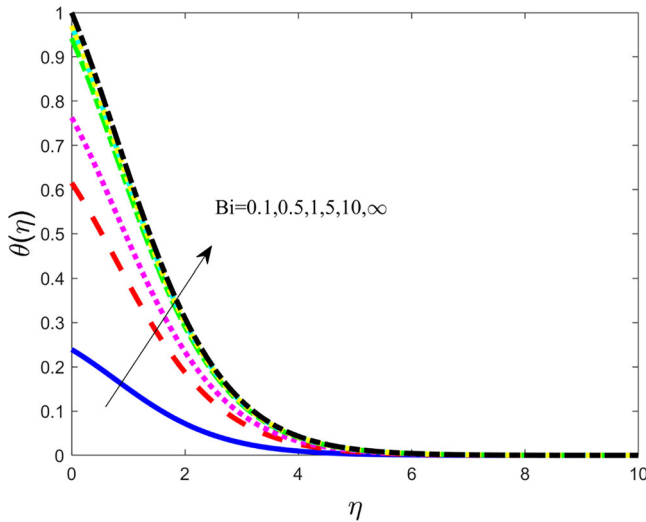

Figure 10. Profiles of 03B8(η) at Pr $= 2$, $\alpha = 0.1$, $\lambda = 0.2$, Nt $=$ Nb $= 0.1$, n $= 1$, Sc $= 0.8$, $\delta = 0.5$, E $= 1$, Lb $=$ Pe $= 1$, N $= 0.1$, Mc $= 0.1$, $\beta = 0.1$.

expression exhibits the variation in the free stream temperature with the impact of absorption coefficients. The enhanced radiation will augment the fluid temperature throughout by enhancing bounding surface thickness. The variation in the profile at the surface is due to the consideration of the heat flux conditions. Figure 9 shows the behavior of the thermal radiation on the concentration distribution and this contribution occurs because of the coupling behavior of the profiles of the temperature and concentration. Though the profile enhances near the surface, the magnitude decreases with increasing radiation, and this exhibits a greater increase in the thickness.

3.4. Effect of thermal Biot number

Figure 10 illustrates the characteristic of the thermal Biot number on the nanofluid temperature distribution for the existence of the other characterizing factors. The assumption of the heat flux
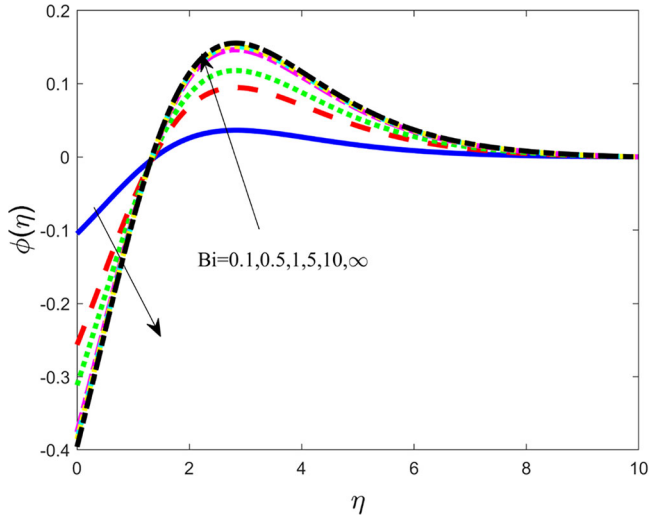
Figure 11. Profiles of $\phi(\eta)$ at Pr $= 2$, $\alpha = 0.1$, $\lambda = 0.2$, Nt $=$ Nb $= 0.1$, n $= 1$, Sc $= 0.8$, $\delta = 0.5$, E $= 1$, Lb $=$ Pe $= 1$, N $= 0.1$, Mc $= 0.1$, $\beta = 0.1$.
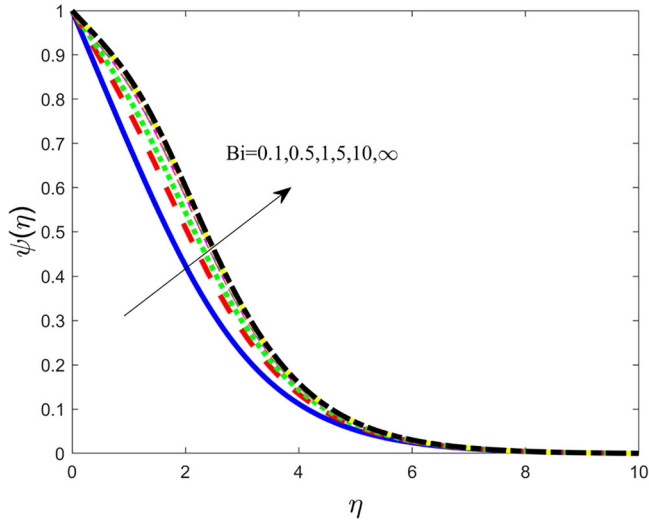

Figure 12. Profiles of $\psi(\eta)$ at Pr $= 2$, $\alpha = 0.1$, $\lambda = 0.2$, Nt $=$ Nb $= 0.1$, n $= 1$, Sc $= 0.8$, $\delta = 0.5$, E $= 1$, Lb $=$ Pe $= 1$, N $= 0.1$, Mc $= 0.1$, $\beta = 0.1$.

boundary condition exhibits the role of the thermal Biot number. The large value of Bi indicates the withdrawal of the flux condition, and this validates the conditions considered herein. Further, the enhanced Biot number is favorable to enhance the fluid temperature that causes a sooth augmentation in the thermal boundary layer thickness. The increasing thickness reveals the movement of the fluid energy from the bottom part, and this causes a greater cooling of the surface. Figure 11 demonstrates the behavior of Bi on the fluid concentration distribution. With an increasing negative magnitude, the fluid concentration retards for the increasing Biot number nearest the surface region up to the meeting point of the profiles at $\eta = 2$ an afterward reverse trend is exhibited in enhancing the profile for the Biot number. A higher value of Bi i.e. $Bi \to \infty$ credits for the nonexistence of heat flux shows maximum enhancement in comparison to other existing values. Moreover, Figure 12 shows the increasing behavior in the profiles of
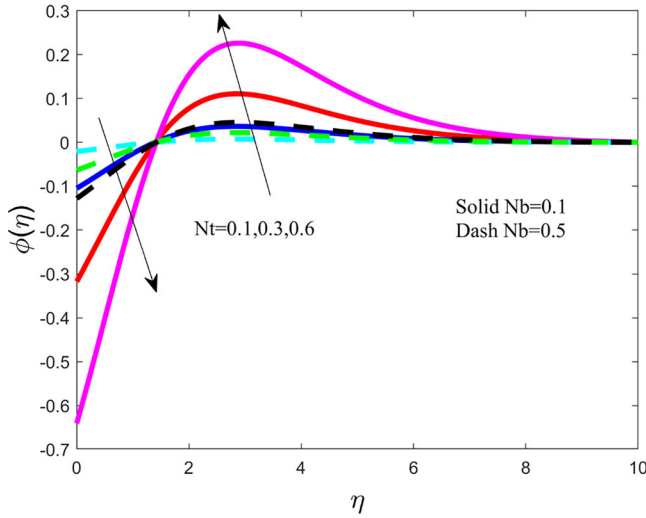
Figure 13. Profiles of $\phi(\eta)$ at Pr $=$ 2, $\alpha=0.1$, $\lambda=0.2$, Bi $=$ 0.1, n$=$1, Sc $=$ 0.8, $\delta=0.5$, E$=$1, Lb$=$Pe $=$ 1, N$=$0.1, Mc $=$ 0.1, $\beta=0.1$.
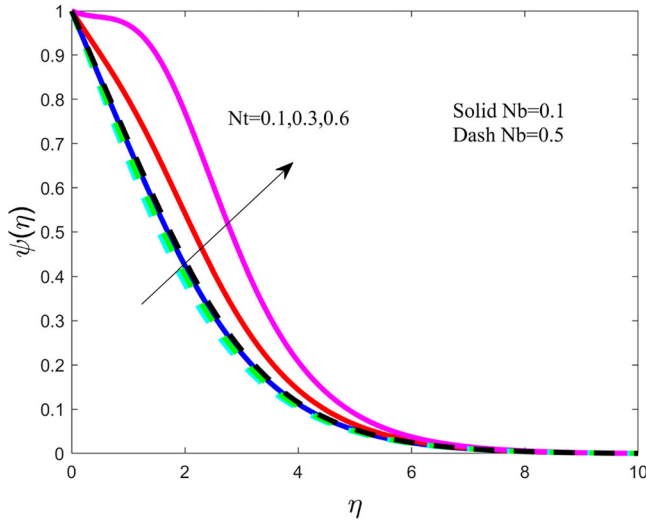
Figure 14. Profiles of $\psi(\eta)$ at Pr $=$ 2, $\alpha=0.1$, $\lambda=0.2$, Bi $=$ 0.1, n$=$1, Sc $=$ 0.8, $\delta=0.5$, E$=$1, Lb$=$Pe $=$ 1, N$=$0.1, Mc $=$ 0.1, $\beta=0.1$.

micro-organisms for the enhanced Biot number. This behavior shows an augmentation in the thickness of the surface with an asymptotic nature.

3.5. The behavior of thermophoresis and Brownian motion

Figure 13 portrays the significant behavior of the thermophoresis affecting the concentration distribution for the variation in the Brownian motion. This observation occurs for the cross-diffusion effect between the profiles of temperature and concentration. Brownian is the measure of the thermal rate within the system due to the random movement of the particles. Also, thermophoresis is the diffusion of thermal energy into the concentration gradient that couples the profiles. The figure exhibits the behavior of Nb their diversified values such as the $Nb = 0.1$ (solid) and $Nb = 0.5$ (Dash). Irrespective of the variation of Nb, the variation of Nt shows dual characteristics
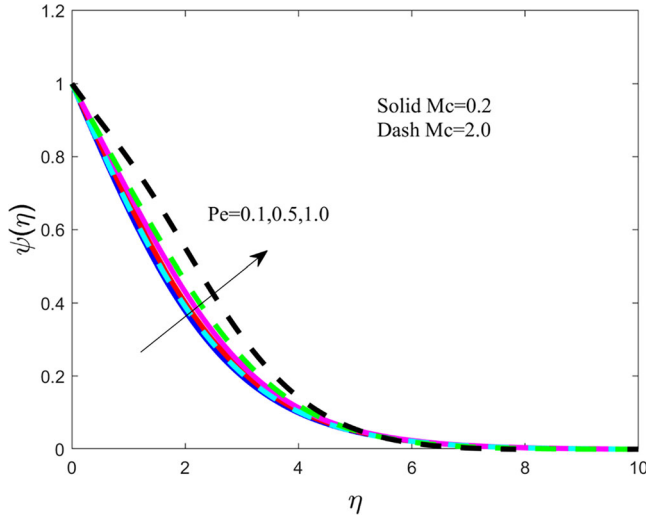
Figure 15. Profiles of $\psi(\eta)$ at $Pr = 2$, $\alpha = 0.1$, $\lambda = 0.2$, $Bi = 0.1$, $Nt = Nb = 0.1$, $n = 1$, $Sc = 0.8$, $\delta = 0.5$, $E = 1$, $Lb = 1$, $N = 0.1$, $\beta = 0.1$.

Table 2. Computation of Nusselt Number for different Values of $\alpha, Bi, N, Nt, \& Nb$ when $Pr = 6.2, n = 0.5$, $\lambda = 0.2$, $Sc = 0.8$, $\delta = 1$, $E = 1$, $L_b = Pe = 1$, $Mc = 0.1$, $\beta = 0.1$.

α	Bi	N	Nt	Nb	$Re_r^{-0.5}Nu$
0.1	0.1	0.1	0.1	0.1	0.094862423
0.3					0.095910450
0.5					0.097184817
0.1	0.5				0.303810226
	2.0				0.511175723
	5.0				0.589642476
	0.1	0.5			0.126265356
		1.0			0.163834844
		1.2			0.199669553
		0.1	0.2		0.094784864
			0.3		0.094705381
			0.5		−0.181148618
			0.1	0.2	0.094862423
				0.3	0.094784864
				0.5	0.094705381

from the point of inflection as depicted in the figure. Near the surface region, the increasing thermophoretic effect attenuates the fluid concentration with increasing magnitude in the negative direction. Further, afterward, the trend shows its opposite impact. In comparative analysis, it is seen that the enhanced Brownian motion favors in enhancing the concentration profile. Figure 14 exhibits the influence of both of these parameters on the motile micro-organism profiles. The profile augments with the increasing factor of the thermophoresis and reverse impact is rendered for the increasing Brownian motion. Finally, Figure 15 displays the impact of peclet number on the motile micro-organism profiles. The profile augments with the increasing the peclet number values.

3.6. The behavior of various components on rate coefficients

The simulated numerical results of the Nusselt number for the diversified parameters within their proper range are depicted in Table 2. The observation reveals that for the enhanced non-Newtonian parameter along with the inclusion of Biot number due to heat flux and thermal radiation augments the heat transfer rate significantly. Further, thermophoresis and Brownian motion

Table 3. Computation of Sherwood number for different Values of $Sc, \delta, E, \sigma_1, n, Nt, \& Nb$ when $Sc = 0.8, Pr = 2, n = 0.5$.

Sc	δ	E	σ_1	n	Nt	Nb	$Re_r^{-0.5} Sh$
0.22	0.5	1.0	1.0	1.0	0.1	0.1	0.076522453
0.78							0.076435664
2.62							0.076313058
0.22	1.0						0.076518334
	1.5						0.076514319
	2.0						0.076510423
	0.5	0.5					0.076518334
		1.5					0.076514319
		2.0					0.076510423
		1.0	1.5				0.076504048
			2.0				0.076491118
			2.5				0.076479315
			1.0	0.5			0.076520695
				1.5			0.076515833
				2.0			0.076513188
				1.0	0.2		0.152892358
					0.3		0.229118589
					0.4		0.305193396
					0.1	0.2	0.038259167
						0.3	0.025506111
						0.4	0.019129584

Table 4. Computation of Deborah Number for different Values of $\alpha, L_b, Pe \& Mc$ when $Pr = 6.2$, $n = 0.5$, $Bi = Nt = Nb = N = 0.1$, $\lambda = 0.2$, $Sc = 0.8$, $\delta = 0.5$, $E = 1$, $\beta = 0.1$.

α	L_b	Pe	Mc	$Re_r^{-0.5} De$
0.1	1.0	1.0	0.1	0.299214497
0.3				0.326365747
0.5				0.365873456
0.1	0.3			0.106820423
	0.6			0.197722825
	0.9			0.275961636
	1.0	0.1		0.360860994
		0.3		0.347035575
		0.5		0.333281546
		1.0	0.2	0.293393305
			0.4	0.281750923
			0.6	0.270108540
			1.0	0.246824716

attenuate the profile of the heat transfer rate. Table 3 shows the significant behavior of the contributing parameters on the Sherwood number. The heavier species favors a declaration in the solutal transfer rate whereas insignificant retardation occurs for the increasing thermal difference and the Arrhenius energy. The enhanced chemical reaction also favors in restricting the coefficient. Dual observation is revealed for the thermophoresis and the Brownian motion on the Sherwood number. It is seen that the solutal rate enhances for the increasing thermophoresis, but it retards significantly for the increasing Brownian motion. Table 4 represents the variation of diversified parameters on the computation of the Deborah number with the existence of other fixed parameters. The increasing behavior of the non-Newtonian parameter enhances the Deborah number along with the variation of the Lewis number. However, increasing Peclet and magnetic parameters retards the Deborah number significantly.

3.7 Response surface Methodology (RSM)

The goal of the RSM is to empirically establish connections between several independent input factors and several distinct output variables. This method is useful for assessing multi-response

Table 5. Range of effective parameters and their levels for Nu.

Parameter	Level		
	Low (−1)	Middle (0)	High (1)
$0.1 < Nt < 0.3$	0.1	0.2	0.3
$0.1 < Bi < 0.5$	0.1	0.3	0.5
$0.5 < N < 1.5$	0.5	1	1.5

processes with several variables since it reveals which input factors have the least and greatest impact on the outcomes. Introducing RSM in 1951, its main purpose was to optimize the response. Using RSM, the influence of selected input parameters Nt, Bi and N on the response variable is examined. As a result of simulation, the range of the parameters is considered to be $0.1 < Nt < 0.3$, $0.1 < Bi < 0.5$, $0.5 < N < 1.5$. Further, a statistical model is developed which consists of 20 runs in sorted order for three independent factors and is documented in Table 5. Table 6 displays the results of a Central Composite Design in short CCD, that uses a face-centered approach to create a second-order model for three input parameters over three levels. This model elucidates the influence of input parameter interactions on the output. The following is the regression model expressed as in terms of a second-order polynomial model for this optimization analysis:

$$Nusselt\ number = 0.228867 - 0.003659\ Nt + 0.067450\ Bi + 0.022064\ N + 0.000250\ Nt^2$$
$$-0.029099\ Bi^2 - 0.004016\ N^2 - 0.002885\ Nt*Bi - 0.000906\ Nt*N - 0.000529\ Bi*N$$

The subsequent outcomes are then obtained by first deleting the irrelevant components from the response function and then figuring out the coefficients of regression.

$$Nu(Nusselt\ number) = 0.228867 - 0.003659Nt + 0.067450Bi + 0.022064N - 0.029099Bi^2$$
$$- 0.004016N^2 - 0.002885NtBi$$

3.8. Analysis of variance for accuracy

For testing of the accuracy of the model, an effective statistical approach i.e. "*Analysis of Variance*" (ANOVA) is used and the results for different sources with corresponding degrees of freedom are presented in Table 7. It also exhibits the results of different testing like p-values, F-values, adjusted sum of squares, adjusted mean square (AMS), errors, and total error. The standard results are obtained with $F - values > 1$ and $p - values < 0.05$ to get the better accuracy of the proposed model with a 5% significant level or 95% confidence. The tabular result reveals for the considered range of Nt, Bi and N the p-values are obtained by ANOVA and the model for the response with these factors is presented. Finally, it is concluded that the designed model is a best-fit model since the resultant table displays the adjusted, as well as computed values, $R^2 = 100\%$. Further, Figure 16 displays the residual plots combined with the regression line as well as the fitting values for their various order, recommending that all the expected values rendered are very much closer to a formation of the straight line.

3.9. Sensitivity analysis

Sensitivity analysis is a key concept in the modeling and simulation of the proposed design. The current study examines the heat transfer rate's sensitivity to small changes in parameters under controlled conditions. It is described as the partial derivative of the response function of the local Nusselt number concerning the characterizing parameters (Nt, Bi, N), also known as (A, B, C) coded variables. This is how you calculate the derivative in partial form for the actual variables.

Table 6. Experimental design for *Nu*.

Runs	Low	Middle	High	*Nt*	*Bi*	*N*	*Nu*
1	−1	−1	−1	0.10	0.10	0.50	0.10713
2	1	−1	−1	0.30	0.10	0.50	0.106415
3	−1	1	−1	0.10	0.50	0.50	0.247166
4	1	1	−1	0.30	0.50	0.50	0.237189
5	−1	−1	1	0.10	0.10	1.50	0.152021
6	1	−1	1	0.30	0.10	1.50	0.14996
7	−1	1	1	0.10	0.50	1.50	0.292218
8	1	1	1	0.30	0.50	1.50	0.276338
9	−1	0	0	0.10	0.30	1.00	0.232883
10	1	0	0	0.30	0.30	1.00	0.224931
11	0	−1	0	0.20	0.10	1.00	0.130997
12	0	1	0	0.20	0.50	1.00	0.268119
13	0	0	−1	0.20	0.30	0.50	0.20064
14	0	0	1	0.20	0.30	1.50	0.248642
15	0	0	0	0.20	0.30	1.00	0.229008
16	0	0	0	0.20	0.30	1.00	0.229008
17	0	0	0	0.20	0.30	1.00	0.229008
18	0	0	0	0.20	0.30	1.00	0.229008
19	0	0	0	0.20	0.30	1.00	0.229008
20	0	0	0	0.20	0.30	1.00	0.229008

Table 7. Analysis of the Variance table for *Nu*.

Source	Degrees of Freedom	Adjusted Sum of Squares	Adjusted Mean Square	F-Value	P-Value	Coefficients
Model	9	0.055539	0.006171	3924.08	0.000	(Constant) 0.228867
Linear	3	0.050497	0.016832	10703.62	0.000	
Nt	1	0.000134	0.000134	85.14	0.000	−0.003659
Bi	1	0.045495	0.045495	28930.19	0.000	0.067450
N	1	0.004868	0.004868	3095.52	0.000	0.022064
Square	3	0.004966	0.001655	1052.66	0.000	
Nt^2	1	0.000000	0.000000	0.11	0.748	0.000250
Bi^2	1	0.002329	0.002329	1480.75	0.000	−0.029099
N^2	1	0.000044	0.000044	28.20	0.000	−0.004016
2-Way Interaction	3	0.000075	0.000025	15.98	0.000	
$Nt \times Bi$	1	0.000067	0.000067	42.33	0.000	−0.002885
$Nt \times N$	1	0.000007	0.000007	4.17	0.068	−0.000906
$Bi \times N$	1	0.000002	0.000002	1.42	0.260	−0.000529
Error	10	0.000016	0.000002			
Lack-of-Fit	5	0.000016	0.000003	*	*	
Pure Error	5	0.000000	0.000000			
Total	19	0.055555				

$R^2 = 99.97\%, Adjusted\ R^2 = 99.95\%$

$$\frac{\partial Nu}{\partial Nt} = -0.003659 - 0.002885 Bi$$

$$\frac{\partial Nu}{\partial Bi} = 0.067450 - 0.058198 Bi - 0.002885 Nt$$

$$\frac{\partial Nu}{\partial N} = 0.022064 - 0.008032 N$$

The sensitivity of the heat flow rate is shown in Table 8 here. The rates of heat transport have increased and decreased, respectively, as seen by both positive and negative numbers. When the rate of change is positive, the parameters and the response variable are positively associated; when the rate of change is negative, they are negatively associated. From the Table it can be observed that the transport of heat toward thermophoresis has the highest sensitivity value (-0.000774) at the uncoded values of $(A = 0, B = -1, C = -1)$ $Nt = 0.2, N = 0.5 \& Bi = 0.1$, toward thermal Biot number has the highest sensitivity value (0.125648) at $Nt = 0.2$,
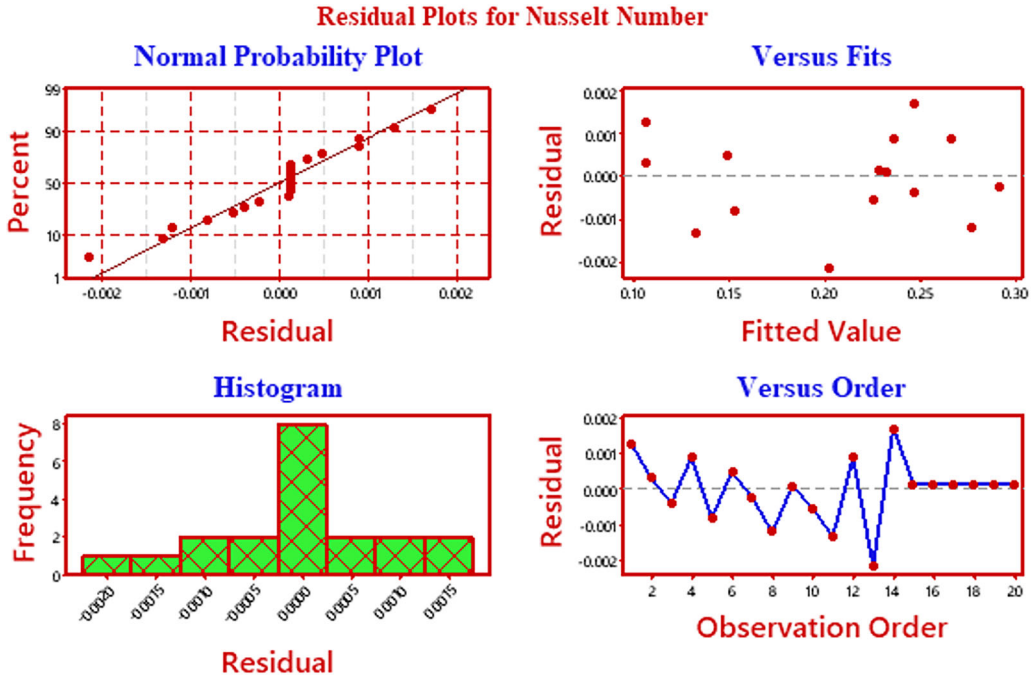
Figure 16. Residual Plots for Nu.

Table 8. Sensitivity analysis of the response Nu.

N	Bi	Sensitivity values		
		$\frac{\partial Nu}{\partial Nt}$	$\frac{\partial Nu}{\partial Bi}$	$\frac{\partial Nu}{\partial N}$
-1	-1	-0.000774	0.125648	0.030096
	0	-0.003659	0.06745	0.030096
	1	-0.006544	0.009252	0.030096
0	-1	-0.000774	0.125648	0.022064
	0	-0.003659	0.06745	0.022064
	1	-0.006544	0.009252	0.022064
1	-1	-0.000774	0.125648	0.014032
	0	-0.003659	0.06745	0.014032
	1	-0.006544	0.009252	0.014032

$N = 0.5\&Bi = 0.1$ and toward thermal radiation has highest sensitivity value at the uncoded values of $Nt = 0.2, N = 1.5\&0.1 < Bi < 0.5$. Similarly, the lowest sensitivity value (-0.006544) of heat transport toward thermophoresis is at the uncoded values of $Nt = 0.2, N = 0.5\&Bi = 0.5$, toward thermal Biot number is (0.009252) at the uncoded values of $Nt = 0.2, N = 0.5\&Bi = 0.5$, and toward thermal radiation is (0.014032) at the uncoded values of $Nt = 0.2, N = 1.5\&0.1 < Bi < 0.5$. The low to higher level values of thermal radiation as well as the thermal Biot number control the rise in the rate of heat transfer but for the low to high-level values N, the rise in the rate of transfer of heat can be achieved at the middle-level values Nt and Bi. Furthermore, the sensitivity toward thermal radiation at the middle level of Nt and lower level values of thermal radiation for the low to high-level values of thermal Biot number remains unchanged.

3.10. Contour and surface plots for the response function

The variation of the various factors like and on the surface and the contour plot for the response of Nusselt number is displayed through Figures 17–22. Figure 17 portrays the impact of the
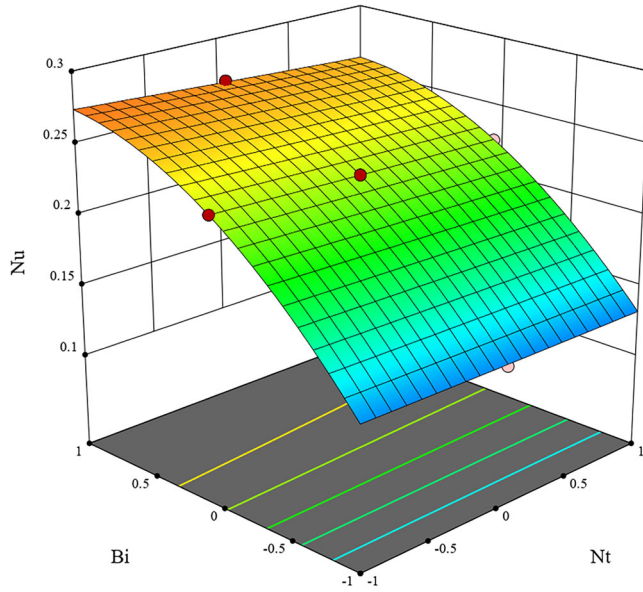
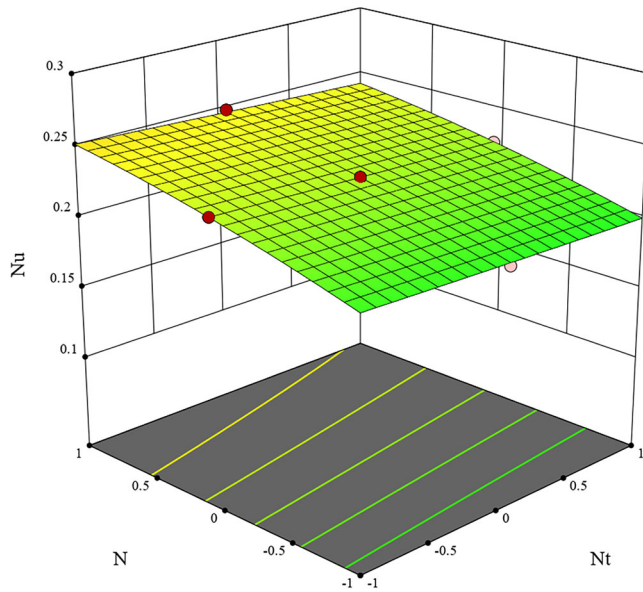**Figure 17.** Surface Plot for the components *Bi* and *Nt* on the response *Nu*.

Figure 18. Surface Plot for the components *N* and *Nt* on the response *Nu*.

interact terms thermophoresis and Biot number on the Nusselt number with the proposed zero level of the third-factor thermal radiation through the surface plot. The observation reflects that the enhanced Biot number augments the heat transfer rate where the variation thermophoresis decreases insignificantly. Figure 18 illustrates the surface plot for the substantial characteristic of the factors of thermal radiation and thermophoresis on the heat transfer rate by ignoring the factor of Biot number. The result shows that enhanced thermal radiation increases the response significantly. Figure 19 depicts the surface plot for the behavior of the factors thermal radiation and the Biot number on the response of heat transfer rate withdrawing the role of the factor thermophoresis. The observation reveals that the variation of both factors augments the rate coefficient
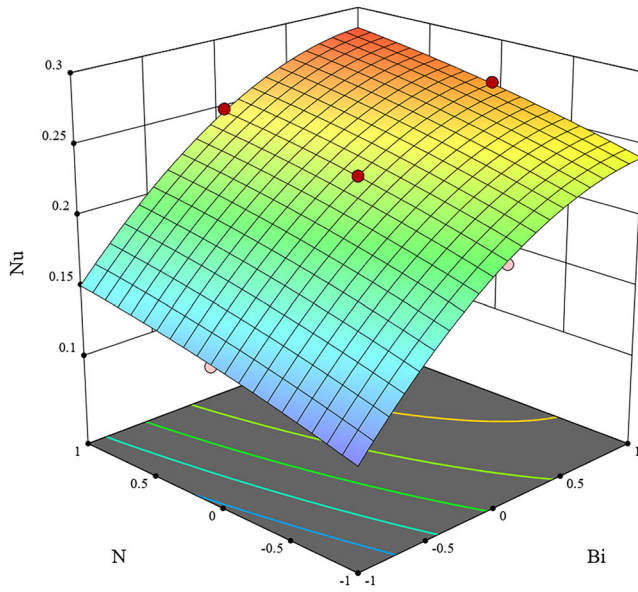
Figure 19. Surface Plot for the components N and Bi on the response Nu.
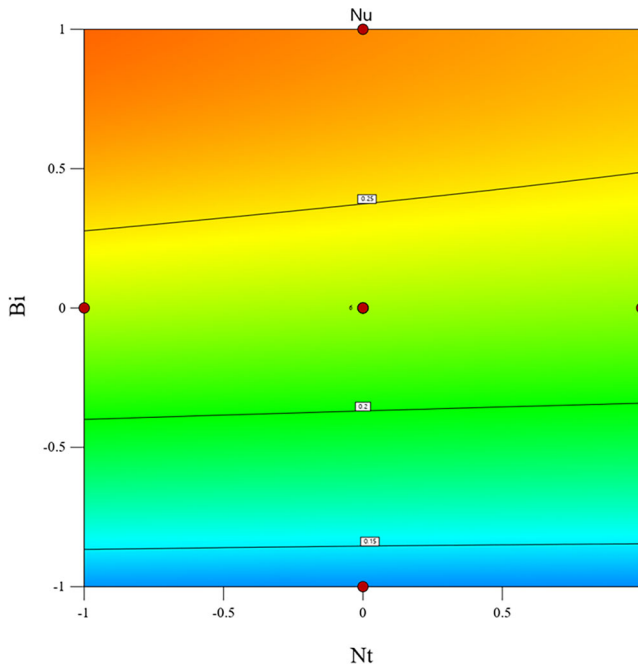
Figure 20. Contour plot for the components Bi and Nt on the response Nu.

throughout. Further, Figure 20 exhibits the pattern of the response of the Nusselt number through the contour plot for the factors thermophoresis and Biot number. It reveals that the flow pattern enhances significantly with the increasing factors. Figure 21 shows the contour plot for the variation of thermal radiation and thermophoresis and the result shows an incredible enhancement in the response for both factors. Finally, Figure 22 portrays the role of thermal radiation and the Biot number on the heat transfer rate *via* a contour plot. A similar tendency is observed for the variation of both these factors.
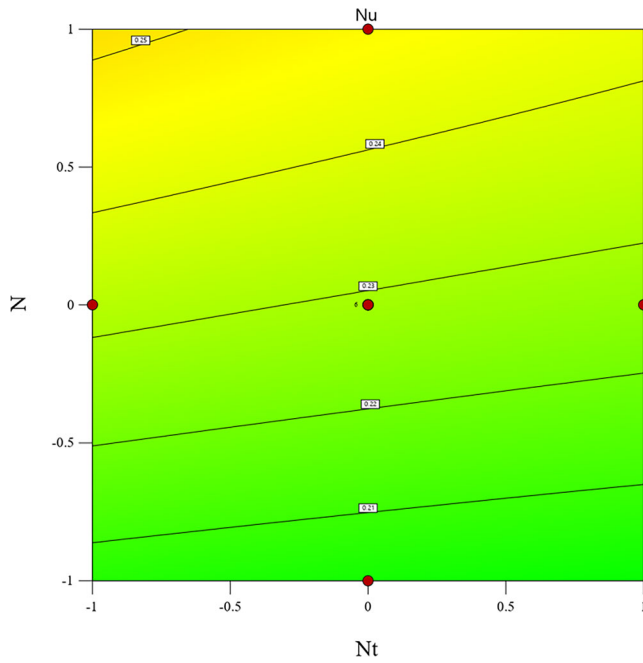
Figure 21. Contour plot for the components N and Nt on the response Nu.
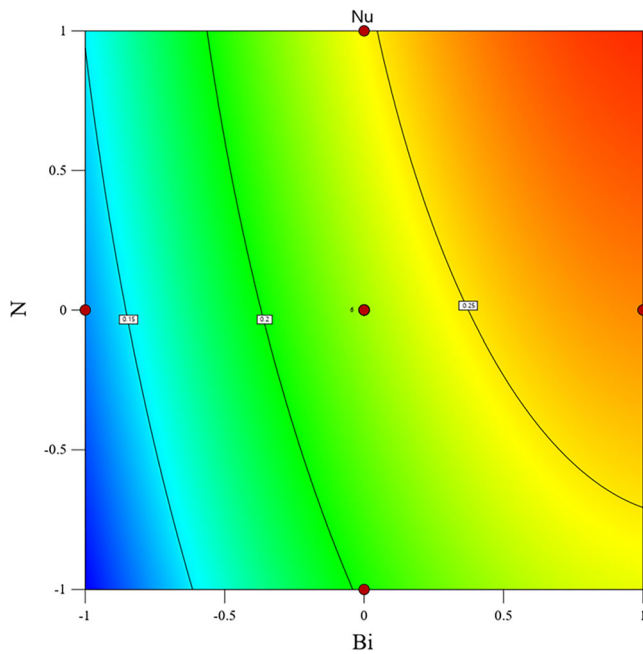
Figure 22. Contour plot for the components N and Bi on the response Nu.

4. Conclusive remarks

The proposed study discloses a statistical approach such as the response surface methodology for the optimization of the heat transfer rate for the bio-convective flow of non-Newtonian nanofluid over a circular disk that is stretching in a radial direction with a uniform rate. The novel

characteristic of a binary chemical reaction and activation energy is incorporated to enhance the study. The regression analysis is accessible through the analysis of variance with sensitivity analysis. Further, the outstanding outcomes are deployed as follows;

- The conformity of the current result of the rate coefficients like heat transfer rate, solutal transfer rate and Deborah number with the earlier established result shows good agreement and that also reveals the convergence criteria of the current methodology.
- The non-Newtonian parameter along with the stretching parameter shows its significant features in enhancing the radial velocity profile further reverse trend is observed in the fluid temperature.
- The radiating heat along with thermal Biot number enriches the nanofluid temperature but the concentration distribution retards the increasing radiation further, the energy created at the surface region stored thereat then boosts up the fluid temperature significantly due to radiation.
- The optimization of the response of the Nusselt number for the various factors i.e. thermal radiation, thermophoresis, and the Biot number is presented using response surface methodology and is validated with the statistical approach of ANOVA with regression analysis.
- Sensitivity analysis confirms that heat transfer rate is positively correlated with thermal radiation and thermal Biot number, but negatively correlated with thermophoresis parameter.

ORCID

Surender Ontela ⓘ http://orcid.org/0000-0003-1006-8255
Venkataramana Musala ⓘ http://orcid.org/0000-0003-0489-6425
Sameh E. Ahmed ⓘ http://orcid.org/0000-0002-5368-5678
Thirupathi Thumma ⓘ http://orcid.org/0000-0002-7993-5647

References

[1]   D.-H. Doh, M. Muthtamilselvan, B. Swathene and E. Ramya, "Homogeneous and heterogeneous reactions in a nanofluid flow due to a rotating disk of variable thickness using HAM," *Math. Comput. Simul.*, vol. 168, pp. 90–110, Feb. 2020. DOI: 10.1016/j.matcom.2019.08.005.

[2]   M. I. Khan, "Transportation of hybrid nanoparticles in forced convective Darcy-Forchheimer flow by a rotating disk," *Int. Commun. Heat Mass Transfer.*, vol. 122, pp. 105177, Mar. 2021. DOI: 10.1016/j.icheatmasstransfer.2021.105177.

[3]   S. Mandal and G. C. Shit, "Entropy analysis on unsteady MHD biviscosity nanofluid flow with convective heat transfer in a permeable radiative stretchable rotating disk," *Chin. J. Phys.*, vol. 74, pp. 239–255, Dec. 2021. DOI: 10.1016/j.cjph.2021.07.036.

[4]   M. K. Nayak, "MHD 3D flow and heat transfer analysis of nanofluid by shrinking surface inspired by thermal radiation and viscous dissipation," *Int. J. Mech. Sci.*, vol. 124-125, pp. 185–193, May 2017. DOI: 10.1016/j.ijmecsci.2017.03.014.

[5]   S. Dinarvand and A. Mahdavi Nejad, "Off-centered stagnation point flow of an experimental-based hybrid nanofluid impinging to a spinning disk with low to high non-alignments," *HFF*, vol. 32, no. 8, pp. 2799–2818, Jun. 2022. DOI: 10.1108/HFF-09-2021-0637/FULL/XML.

[6]   E. Ragupathi, D. Prakash, M. Muthtamilselvan and Q. M. Al-Mdallal, "Impact of thermal nonequilibrium on flow through a rotating disk with power law index in porous media occupied by Ostwald-de-Waele nanofluid," *J. Non-Equilibrium Thermodyn.*, vol. 47, no. 4, pp. 375–394, Oct. 2022. DOI: 10.1515/JNET-2022-0030/MACHINEREADABLECITATION/RIS.

[7]   M. Izady, S. Dinarvand, I. Pop and A. J. Chamkha, "Flow of aqueous Fe2O3–CuO hybrid nanofluid over a permeable stretching/shrinking wedge: a development on Falkner–Skan problem," *Chin. J. Phys.*, vol. 74, pp. 406–420, Dec. 2021. DOI: 10.1016/j.cjph.2021.10.018.

[8]   E. A. Algehyne, N. H. Altaweel, A. Saeed, A. Dawar, M. Ramzan, and P. Kumam, "A semi-analytical passive strategy to examine the water-ethylene glycol (50:50)-based hybrid nanofluid flow over a spinning disk with homogeneous–heterogeneous reactions," *Sci. Rep.*, vol. 12, no. 1, pp. 17105, Oct. 2022. DOI: 10.1038/s41598-022-21080-z.

[9] M. K. Sarangi, D. N. Thatoi, S. Shaw, M. Azam, A. J. Chamkha and M. K. Nayak, "Hydrothermal behavior and irreversibility analysis of Bödewadt flow of radiative and dissipative ternary composite nanomaterial due to a stretched rotating disk," *Materials Sci. Engineering: b*, vol. 287, pp. 116124, Jan. 2023. DOI: 10.1016/j.mseb.2022.116124.

[10] S. Dinarvand and M. N. Rostami, "Three-dimensional squeezed flow of aqueous magnetite–graphene oxide hybrid nanofluid: a novel hybridity model with analysis of shape factor effects," *Proc. Institut. Mech. Engineers, Part E: J. Process Mech. Engng.*, vol. 234, no. 2, pp. 193–205, 2020. DOI: 10.1177/0954408920906274.

[11] S. E. Ahmed, A. A. M. Arafa and S. A. Hussein, "Bioconvective flow of a variable properties hybrid nano-fluid over a spinning disk with Arrhenius activation energy, Soret and Dufour impacts," *Numer. Heat Transfer, Part A: Applicat.*, pp. 1–23, 2023. DOI: 10.1080/10407782.2023.2193709.

[12] M. D. Shamshuddin et al., "MHD bioconvection microorganism nanofluid driven by a stretchable plate through porous media with an induced heat source," *Waves Random Complex Media*, pp. 1–25, 2022. DOI: 10.1080/17455030.2022.2126024.

[13] P. P. Humane, V. S. Patil, M. D. Shamshuddin, G. R. Rajput and A. B. Patil, "Role of bioconvection on the dynamics of chemically active Casson nanofluid flowing via an inclined porous stretching sheet with convective conditions," *Int. J. Modelling Simulation*, pp. 1–20, 2023. DOI: 10.1080/02286203.2022.2164156.

[14] A. R. Bestman, "Natural convection boundary layer with suction and mass transfer in a porous medium," *Int. J. Energy Res.*, vol. 14, no. 4, pp. 389–396, 1990. DOI: 10.1002/er.4440140403.

[15] M. K. Nayak, F. Mabood, A. S. Dogonchi and W. A. Khan, "Electromagnetic flow of SWCNT/MWCNT suspensions with optimized entropy generation and cubic auto catalysis chemical reaction," *Int. Commun. Heat Mass Transfer*, vol. 120, pp. 104996, Jan. 2021. DOI: 10.1016/j.icheatmasstransfer.2020.104996.

[16] Z. Shafique, M. Mustafa and A. Mushtaq, "Boundary layer flow of Maxwell fluid in rotating frame with binary chemical reaction and activation energy," *Results Phys.*, vol. 6, pp. 627–633, 2016. DOI: 10.1016/j.rinp.2016.09.006.

[17] F. Mabood, M. K. Nayak and A. J. Chamkha, "Heat transfer on the cross flow of micropolar fluids over a thin needle moving in a parallel stream influenced by binary chemical reaction and Arrhenius activation energy," *Eur. Phys. J. Plus.*, vol. 134, no. 9, pp. 1–12, 2019. DOI: 10.1140/epjp/i2019-12716-9.

[18] M. Ijaz, M. Ayub and H. Khan, "Entropy generation and activation energy mechanism in nonlinear radiative flow of Sisko nanofluid: rotating disk," *Heliyon*, vol. 5, no. 6, pp. e01863, 2019. DOI: 10.1016/j.heliyon.2019.e01863.

[19] M. K. Nayak, "Chemical reaction effect on MHD viscoelastic fluid over a stretching sheet through porous medium," *Meccanica*, vol. 51, no. 8, pp. 1699–1711, Aug. 2016. DOI: 10.1007/S11012-015-0329-3/METRICS.

[20] Y. M. Chu et al., "Significance of activation energy, bio-convection and magnetohydrodynamic in flow of third grade fluid (non-Newtonian) towards stretched surface: a Buongiorno model analysis," *Int. Commun. Heat Mass Transfer.*, vol. 118, pp. 104893, Nov. 2020. DOI: 10.1016/j.icheatmasstransfer.2020.104893.

[21] T. Hayat, A. A. Khan, F. Bibi and S. Farooq, "Activation energy and non-Darcy resistance in magneto peristalsis of Jeffrey material," *J. Phys. Chem. Solids*, vol. 129, pp. 155–161, 2019. DOI: 10.1016/j.jpcs.2018.12.044.

[22] S. Ahmad, M. Farooq, A. Anjum and N. A. Mir, "Squeezing flow of convectively heated fluid in porous medium with binary chemical reaction and activation energy," *Adv. Mech. Engng.*, vol. 11, no. 10, pp. 168781401988377, 2019. DOI: 10.1177/1687814019883774.

[23] F. Mabood, T. Muhammad, M. K. Nayak, H. Waqas and O. D. Makinde, "EMHD flow of non-Newtonian nanofluids over thin needle with Robinson's condition and Arrhenius pre-exponential factor law," *Phys. Scr.*, vol. 95, no. 11, pp. 115219, Oct. 2020. DOI: 10.1088/1402-4896/abc0c3.

[24] K. Jabeen, "Bioconvective Carreau nanofluid flow with magnetic dipole, viscous, and ohmic dissipation effects subject to Arrhenius activation energy," *Numer. Heat Transfer, Part A: Applicat.*, pp. 1–26, 2023. DOI: 10.1080/10407782.2023.2221005.

[25] N. Acharya and K. Das, "Three-dimensional rotating flow of Cu–Al2O3/kerosene oil hybrid nanofluid in presence of activation energy and thermal radiation," *Numer. Heat Transfer, Part A: Applicat.*, vol. 84, no. 6, pp. 586–603, 2023. DOI: 10.1080/10407782.2022.2147111.

[26] M. Faiz et al., "Multiple slip effects on time dependent axisymmetric flow of magnetized Carreau nanofluid and motile microorganisms," *Sci. Rep.*, vol. 12, no. 1, pp. 14259, 2022. DOI: 10.1038/s41598-022-18344-z.

[27] M. S. Alqarni, S. Yasmin, H. Waqas and S. A. Khan, "Recent progress in melting heat phenomenon for bio-convection transport of nanofluid through a lubricated surface with swimming microorganisms," *Sci. Rep.*, vol. 12, no. 1, pp. 8447, May 2022. DOI: 10.1038/s41598-022-12230-4.

[28] A. Shafiq, A. B. Çolak and T. N. Sindhu, "Optimization of bioconvective magnetized Walter's B nanofluid flow towards a cylindrical disk with artificial neural networks," *Lubricants*, vol. 10, no. 9, pp. 209, Aug. 2022. DOI: 10.3390/lubricants10090209.

[29] S. Dinarvand, S. M. Mousavi, M. Yousefi and M. Nademi Rostami, "MHD flow of MgO-Ag/water hybrid nanofluid past a moving slim needle considering dual solutions: an applicable model for hot-wire anemometer analysis," *HFF*, vol. 32, no. 2, pp. 488–510, Jan. 2022. DOI: 10.1108/HFF-01-2021-0042/FULL/XML.

[30] F. Wang, S. Ahmad, Q. Al Mdallal, M. Alammari, M. N. Khan and A. Rehman, "Natural bio-convective flow of Maxwell nanofluid over an exponentially stretching surface with slip effect and convective boundary condition," *Sci. Rep.*, vol. 12, no. 1, pp. 2220, Feb. 2022. DOI: 10.1038/s41598-022-04948-y.

[31] S. Mandal, G. C. Shit, S. Shaw and O. D. Makinde, "Entropy analysis of thermo-solutal stratification of nanofluid flow containing gyrotactic microorganisms over an inclined radiative stretching cylinder," *Thermal Sci. Engng. Progress*, vol. 34, pp. 101379, Sep. 2022. DOI: 10.1016/j.tsep.2022.101379.

[32] J. Cui, S. Munir, S. F. Raies, U. Farooq and R. Razzaq, "Non-similar aspects of heat generation in bioconvection from flat surface subjected to chemically reactive stagnation point flow of Oldroyd-B fluid," *Alexandria Engng. J.*, vol. 61, no. 7, pp. 5397–5411, Jul. 2022. DOI: 10.1016/j.aej.2021.10.056.

[33] A. Ghasemian, S. Dinarvand, A. Adamian and M. A. Sheremet, "Unsteady General Three-Dimensional Stagnation Point Flow of a Maxwell/Buongiorno Non-Newtonian Nanofluid," *J. Nanofluids*, vol. 8, no. 7, pp. 1544–1559, 2019. Jul DOI: 10.1166/jon.2019.1701.

[34] S. Dinarvand, H. Berrehal, I. Pop and A. J. Chamkha, "Blood-based hybrid nanofluid flow through converging/diverging channel with multiple slips effect: a development of Jeffery-Hamel problem," *HFF*, vol. 33, no. 3, pp. 1144–1160, Jan. 2023. DOI: 10.1108/HFF-08-2022-0489/FULL/XML.

[35] L. Ali, B. Ali, X. Liu, S. Ahmed and M. A. Shah, "Analysis of bio-convective MHD Blasius and Sakiadis flow with Cattaneo-Christov heat flux model and chemical reaction," *Chinese J. Physics*, vol. 77, pp. 1963–1975, Jun. 2022. DOI: 10.1016/j.cjph.2021.12.008.

[36] Y.-Q. Song *et al.*, "Aspects of thermal diffusivity and melting phenomenon in Carreau nanofluid flow confined by nonlinear stretching cylinder with convective Marangoni boundary constraints," *Math. Comput. Simul.*, vol. 195, pp. 138–150, May 2022. DOI: 10.1016/j.matcom.2022.01.001.

[37] B. Mahanthesh, S. A. Shehzad, J. Mackolil and N. S. Shashikumar, "Heat transfer optimization of hybrid nanomaterial using modified Buongiorno model: a sensitivity analysis," *Int. J. Heat Mass Transf.*, vol. 171, pp. 121081, Jun. 2021. DOI: 10.1016/j.ijheatmasstransfer.2021.121081.

[38] M. Saraswathy, D. Prakash, M. Muthtamilselvan and Q. M. Al Mdallal, "Arrhenius energy on asymmetric flow and heat transfer of micropolar fluids with variable properties: a sensitivity approach," *Alexandria Engng J.*, vol. 61, no. 12, pp. 12329–12352, Dec. 2022. DOI: 10.1016/j.aej.2022.06.015.

[39] B. Mahanthesh, J. Mackolil and S. M. Mallikarjunaiah, "Response surface optimization of heat transfer rate in Falkner-Skan flow of $ZnO - EG$ nanoliquid over a moving wedge: sensitivity analysis," *Int. Commun. Heat Mass Transfer.*, vol. 125, pp. 105348, Jun. 2021. DOI: 10.1016/j.icheatmasstransfer.2021.105348.

[40] P. Rana, B. Mahanthesh, K. Thriveni and T. Muhammad, "Significance of aggregation of nanoparticles, activation energy, and Hall current to enhance the heat transfer phenomena in a nanofluid: a sensitivity analysis," *Waves Random Complex Media*, pp. 1–23, 2022. DOI: 10.1080/17455030.2022.2065043.

[41] B. Mahanthesh, K. Thriveni, P. Rana and T. Muhammad, "Radiative heat transfer of nanomaterial on a convectively heated circular tube with activation energy and nanoparticle aggregation kinematic effects," *Int. Commun. Heat Mass Transfer.*, vol. 127, pp. 105568, Oct. 2021. DOI: 10.1016/j.icheatmasstransfer.2021.105568.

[42] P. Rana and G. Gupta, "Sensitivity computation of Von Kármán's swirling flow of nanoliquid under nonlinear Boussinesq approximation over a rotating disk with Stefan blowing and multiple slip effects," *Waves Random Complex Media*, pp. 1–31, 2022. DOI: 10.1080/17455030.2022.2112633.

[43] J. Mackolil and B. Mahanthesh, "Computational simulation of surface tension and gravitation-induced convective flow of a nanoliquid with cross-diffusion: an optimization procedure," *Appl. Math. Comput.*, vol. 425, pp. 127108, Jul. 2022. DOI: 10.1016/j.amc.2022.127108.

[44] P. Rana and G. Gupta, "FEM solution to quadratic convective and radiative flow of Ag-MgO/H2O hybrid nanofluid over a rotating cone with Hall current: optimization using Response Surface Methodology," *Math. Comput. Simul.*, vol. 201, pp. 121–140, Nov. 2022. DOI: 10.1016/j.matcom.2022.05.012.

[45] M. M. Fayyadh *et al.*, "The mathematical model for heat transfer optimization of Carreau fluid conveying magnetized nanoparticles over a permeable surface with activation energy using response surface methodology," *ZAMM - J. Appl. Math. Mech./Zeitschrift Für Angewandte Mathematik Und Mechanik*, vol. 102, no. 11, pp. e202100185, Nov. 2022. DOI: 10.1002/ZAMM.202100185.

[46] P. Rana and A. Kumar, "Nonlinear buoyancy driven flow of hybrid nanoliquid past a spinning cylinder with quadratic thermal radiation," *Int. Commun. Heat Mass Transfer.*, vol. 139, pp. 106439, Dec. 2022. DOI: 10.1016/j.icheatmasstransfer.2022.106439.

[47] A. Abbasi, F. Mabood, W. Farooq and M. Batool, "Bioconvective flow of viscoelastic Nanofluid over a convective rotating stretching disk," *Int. Commun. Heat Mass Transfer.*, vol. 119, pp. 104921, Dec. 2020. DOI: 10.1016/j.icheatmasstransfer.2020.104921.

[48] B. Mahanthesh, G. Lorenzini, F. M. Oudina and I. L. Animasaun, "Significance of exponential space- and thermal-dependent heat source effects on nanofluid flow due to radially elongated disk with Coriolis and Lorentz forces," *J. Therm. Anal. Calorim.*, vol. 141, no. 1, pp. 37–44, Jul. 2020. DOI: 10.1007/s10973-019-08985-0.

[49] U. Khan, S. Bilal, A. Zaib, O. D. Makinde and A. Wakif, "Numerical simulation of a nonlinear coupled differential system describing a convective flow of Casson gold–blood nanofluid through a stretched rotating

rigid disk in the presence of Lorentz forces and nonlinear thermal radiation," *Numer. Methods Partial Differ. Equ.*, vol. 38, no. 3, pp. 22620, Nov. 2020. DOI: 10.1002/num.22620.

[50]   R. S. Rivlin, "Further remarks on the stress-deformation relations for isotropic materials," *J. Rational Mech. Anal.*, vol. 4, pp. 681–702, 1955. https://www.jstor.org/stable/24900379 (accessed Nov. 30, 2022).

[51]   J. E. Dunn and R. L. Fosdick, "Thermodynamics, stability, and boundedness of fluids of complexity 2 and fluids of second grade," *Arch. Rational Mech. Anal.*, vol. 56, no. 3, pp. 191–252, Sep. 1974. DOI: 10.1007/BF00280970/METRICS.

[52]   D. A. Nield and A. V. Kuznetsov, "Thermal instability in a porous medium layer saturated by a nanofluid: A revised model," *Int. J. Heat Mass Transf.*, vol. 68, pp. 211–214, Jan. 2014. DOI: 10.1016/j.ijheatmasstransfer.2013.09.026.

[53]   A. V. Kuznetsov and D. A. Nield, "Natural convective boundary-layer flow of a nanofluid past a vertical plate," *Int. J. Thermal Sci.*, vol. 49, no. 2, pp. 243–247, Feb. 2010. DOI: 10.1016/j.ijthermalsci.2009.07.015.